# Supporting Information

# Normal load and counter body size influence the initiation of microstructural discontinuities in copper during sliding

F. Ruebeling[1,2], Y. Xu[3,4], G. Richter[5], D. Dini[4], P. Gumbsch[1,6], C. Greiner[1,2*]

[1] Karlsruhe Institute of Technology (KIT), Institute for Applied Materials (IAM), Kaiserstrasse 12, 76131 Karlsruhe, Germany
[2] KIT IAM-CMS MicroTribology Center (μTC), Strasse am Forum 5, 76131 Karlsruhe, Germany
[3] Department of Materials, Imperial College London, South Kensington Campus, Exhibition Road, London SW7 2AZ, UK
[4] Department of Mechanical Engineering, Imperial College London, South Kensington Campus, Exhibition Road, London SW7 2AZ, UK
[5] Max Planck Institute for Intelligent Systems (MPI-IS), Heisenbergstrasse 3, 70569 Stuttgart, Germany
[6] Fraunhofer Institute for Mechanics of Materials (IWM), Woehlerstrasse 11, 79108 Freiburg, Germany

[*] Corresponding Author: Christian Greiner, christian.greiner@kit.edu

**Figure S1: TKD patterns in ND and SD and the deviations of the rotation axis to the ND- and SD-axis.** (a) $F_n$ = 2 N, $d_{sphere}$ = 10 mm ($p_{Hertz}$ = 530 MPa), (b) $F_n$ = 5 N, $d_{sphere}$ = 10 mm ($p_{Hertz}$ = 719 MPa), (c) $F_n$ = 6.75 N, $d_{sphere}$ = 10 mm ($p_{Hertz}$ = 795 MPa), (d) $F_n$ = 100 N, $d_{sphere}$ = 10 mm ($p_{Hertz}$ = 1953 MPa), (e) $F_n$ = 1 N, $d_{sphere}$ = 1 mm ($p_{Hertz}$ = 1953 MPa). The given angles within the maps refer to the deviation of the rotation axis to the ND- and SD-axis. All major misorientations are concentrated at the DTL and to a lesser extend at the subgrain boundaries. In comparison to TD (see **Fig. 3** and **Fig. 4**), the patterns reveal a clear change in the crystallographic orientation.

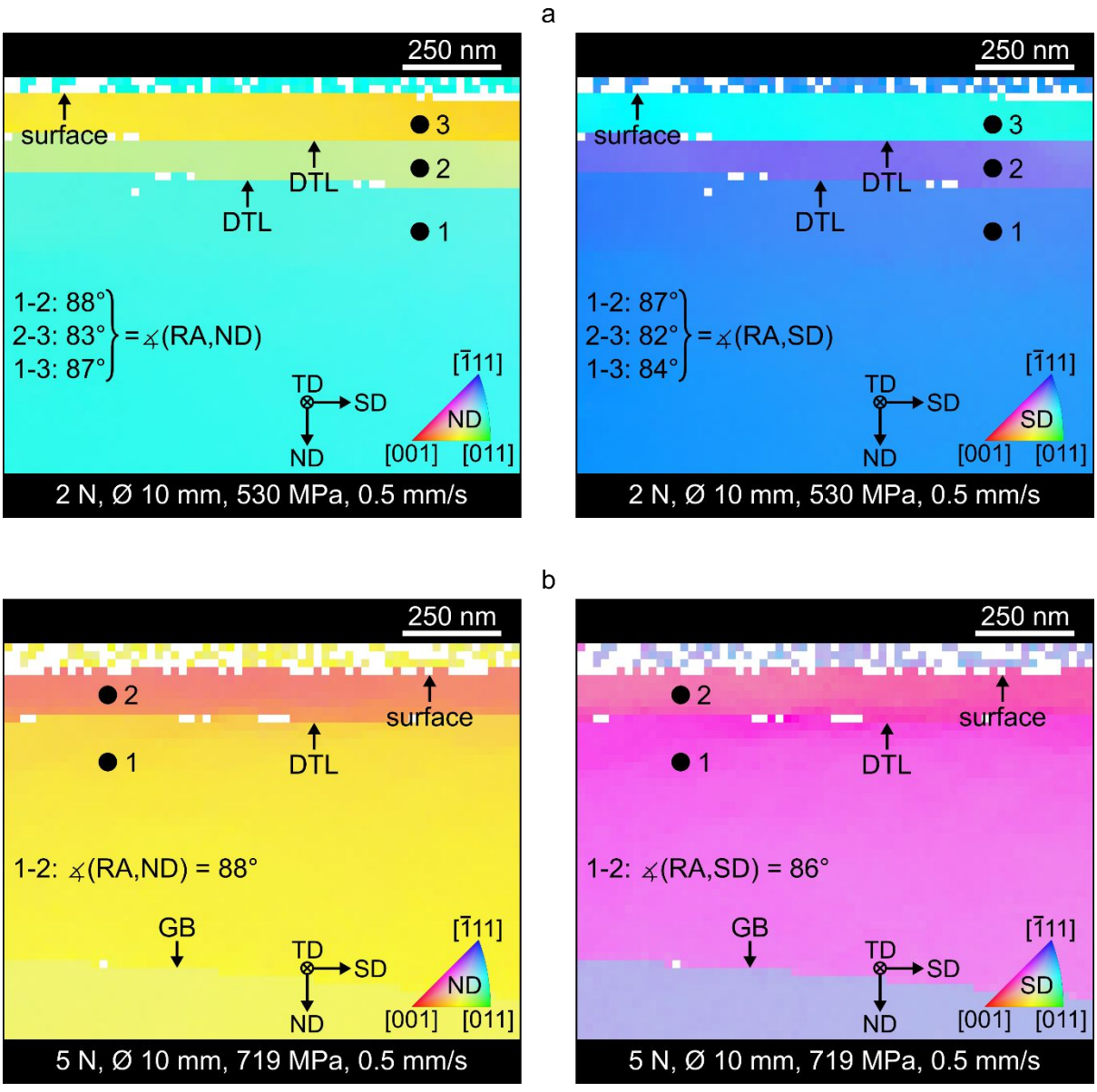

c

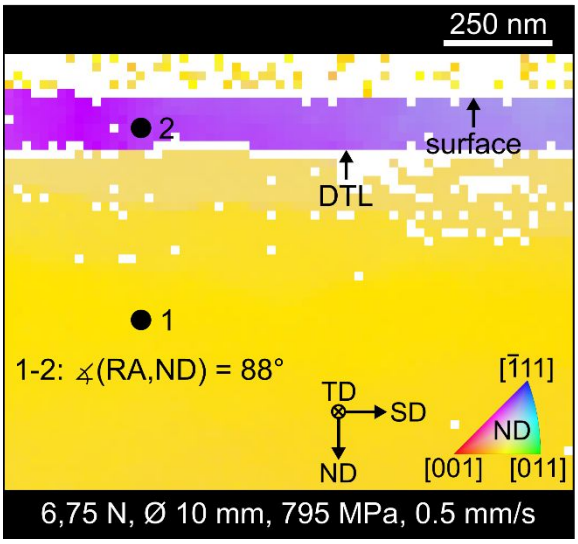
250 nm
2
surface
DTL
1
1-2: ∡(RA,ND) = 88°
TD
SD
ND
[1̄11]
ND
[001] [011]
6,75 N, Ø 10 mm, 795 MPa, 0.5 mm/s

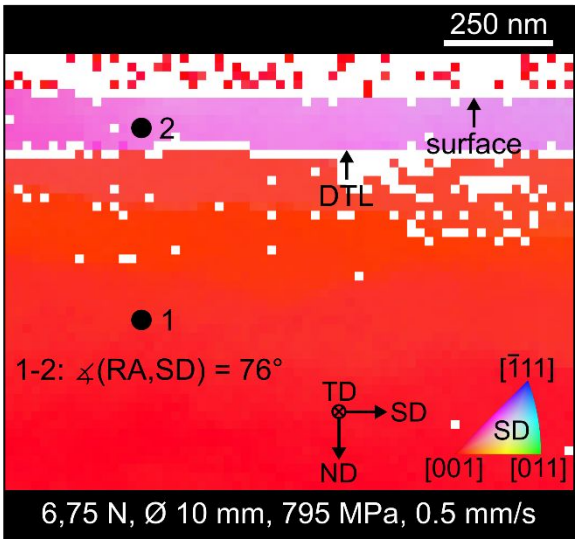
250 nm
2
surface
DTL
1
1-2: ∡(RA,SD) = 76°
TD
SD
ND
[1̄11]
SD
[001] [011]
6,75 N, Ø 10 mm, 795 MPa, 0.5 mm/s

d

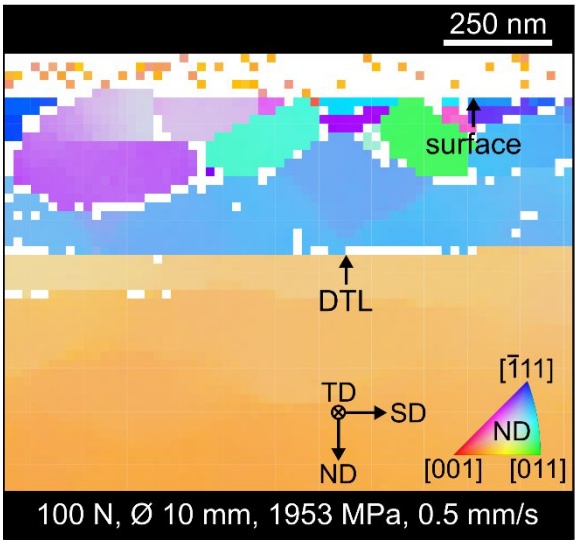
250 nm
surface
DTL
TD
SD
ND
[1̄11]
ND
[001] [011]
100 N, Ø 10 mm, 1953 MPa, 0.5 mm/s

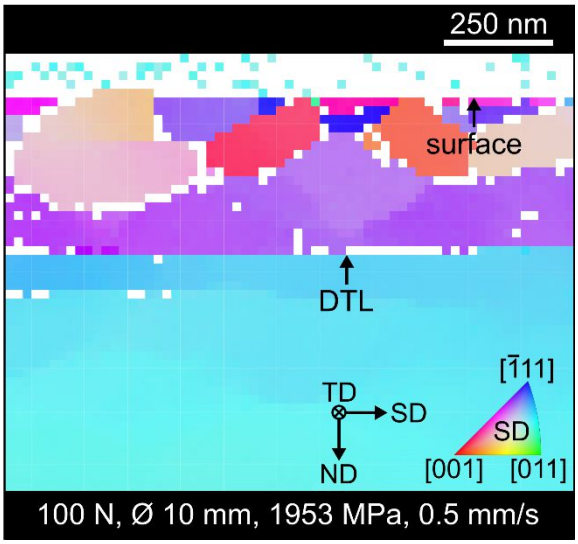
250 nm
surface
DTL
TD
SD
ND
[1̄11]
SD
[001] [011]
100 N, Ø 10 mm, 1953 MPa, 0.5 mm/s

e

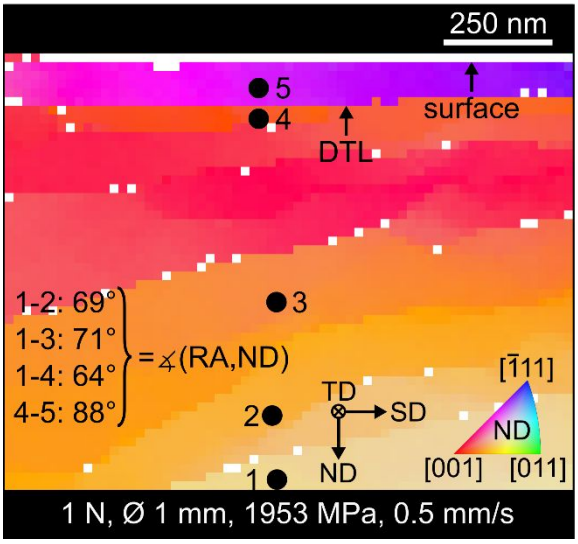
250 nm
5
4
surface
DTL
1-2: 69°
1-3: 71°
1-4: 64°
4-5: 88°
=∡(RA,ND)
3
2
1
TD
SD
ND
[1̄11]
ND
[001] [011]
1 N, Ø 1 mm, 1953 MPa, 0.5 mm/s

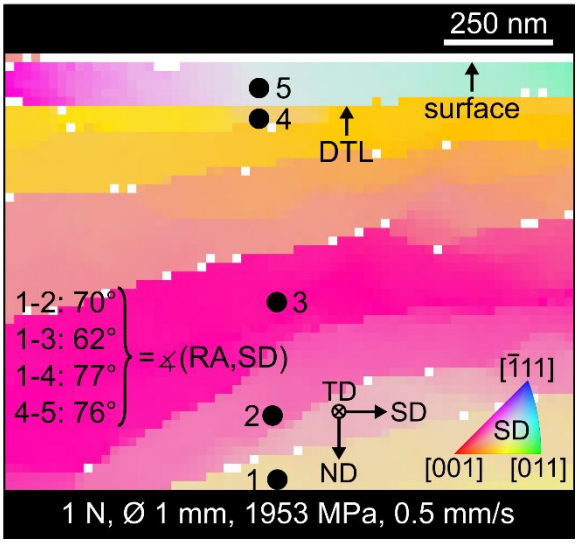
250 nm
5
4
surface
DTL
1-2: 70°
1-3: 62°
1-4: 77°
4-5: 76°
=∡(RA,SD)
3
2
1
TD
SD
ND
[1̄11]
SD
[001] [011]
1 N, Ø 1 mm, 1953 MPa, 0.5 mm/s

**Figure S2: TEM images from the specimen for $F_n$ = 2 N, $d_{sphere}$ = 10 mm ($p_{Hertz}$ = 530 MPa).** (a) bright field image and (b) SAD pattern of the region marked by a dashed circle in the bright field image, (c) dark field image of diffraction spot 1, (d) dark field image using diffraction spot 1 and 2. The continuous white arrow in (b) corresponds to one of the main diffraction spots, whereas two of the secondary diffraction spots are represented by dashed white arrows. The SAD pattern reveals a lattice rotation within the TEM foil. The misorientation between the area directly above and below the DTL is about 13° for the upper DTL and around 12° for the deeper one. The given misorientations refer to the selected zone axis, which was aligned nearly parallel to TD. The zone axis for imaging was [110].

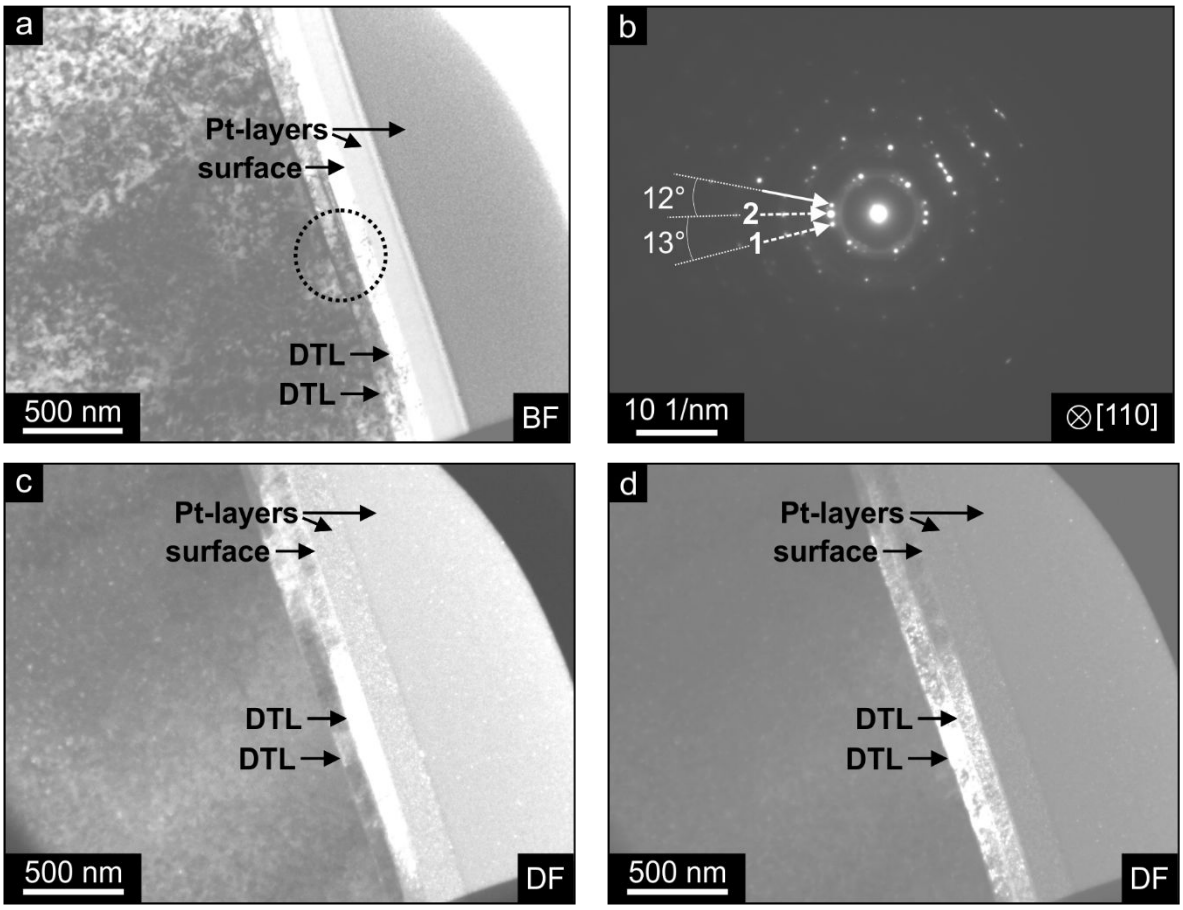

**Figure S3: TEM images from the specimen for $F_n$ = 5 N, $d_{sphere}$ = 10 mm ($p_{Hertz}$ = 719 MPa).** (a) bright field image and (b) SAD pattern of the region marked by a dashed circle in the bright field image, (c) dark field image of diffraction spot 1, (d) dark field image of diffraction spot 2. The continuous white arrow corresponds to one of the main diffraction spots, whereas one of the secondary diffraction spots is represented by the dashed white arrow. The main diffraction spots belong to the less deformed bulk material (c), whereas the secondary diffraction spots refer to the strongly deformed microstructure right underneath the surface (d). The SAD pattern reveals a lattice rotation within the TEM foil. The latter was determined to 10° by measuring the angle between the continuous (1) and the dashed (2) arrow. The given misorientations refer to the selected zone axis, which was aligned nearly parallel to TD. The zone axis for imaging was [110].

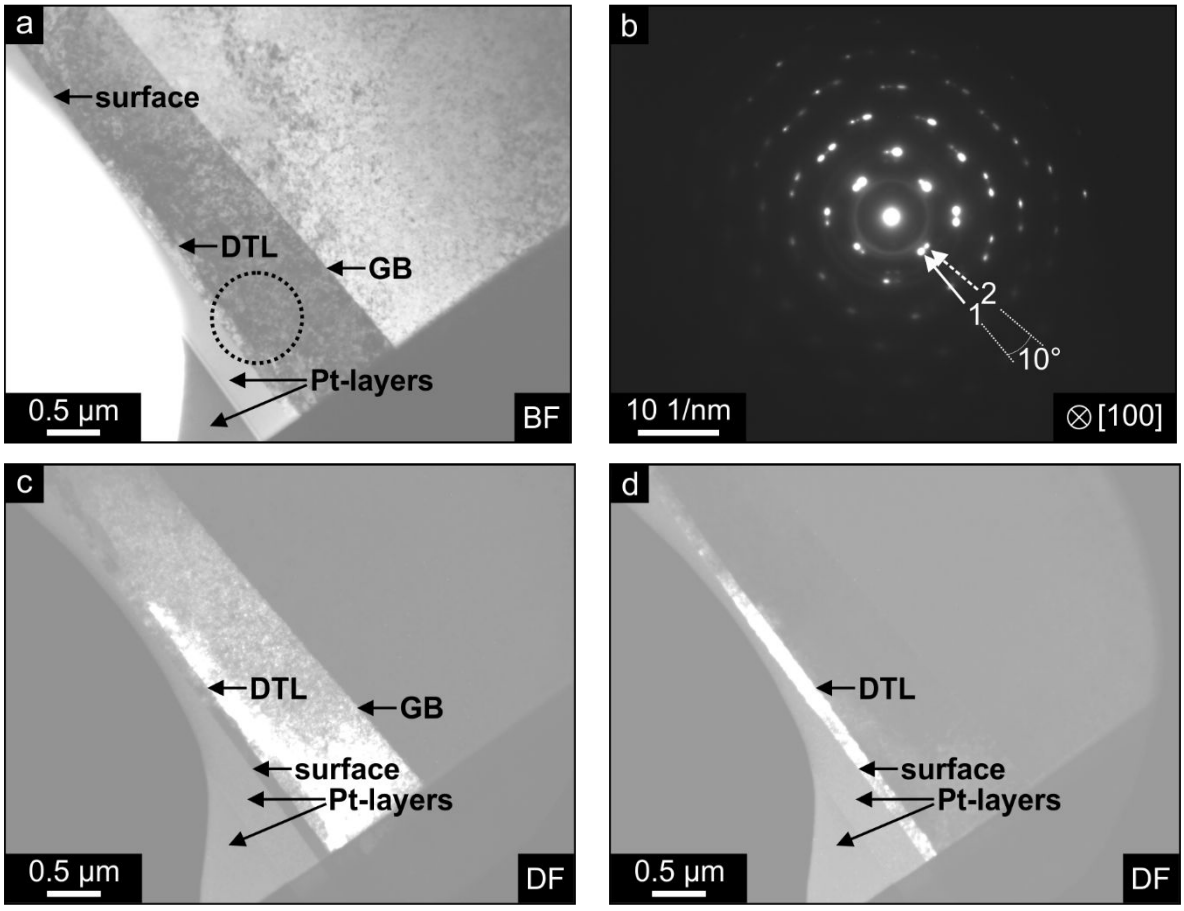

**Figure S4: TEM images from the specimen for $F_n$ = 6.75 N, $d_{sphere}$ = 10 mm ($p_{Hertz}$ = 795 MPa).** (a) bright field image and (b) SAD pattern of the region marked by a dashed circle in the bright field image, (c) dark field image of diffraction spot 1, (d) dark field image of diffraction spot 2. The continuous white arrow in (b) corresponds to one of the main diffraction spots, whereas one of the secondary diffraction spots is represented by the dashed white arrow. The main diffraction spots belong to the less deformed bulk material (c), whereas the diffraction spots refer to the strongly deformed microstructure right underneath the surface (d). The SAD pattern reveals a lattice rotation within the TEM foil. The latter was determined to 20° by measuring the angle between the continuous (1) and the dashed arrow (2). The given misorientations refer to the selected zone axis, which was aligned nearly parallel to TD. The zone axis is [111].

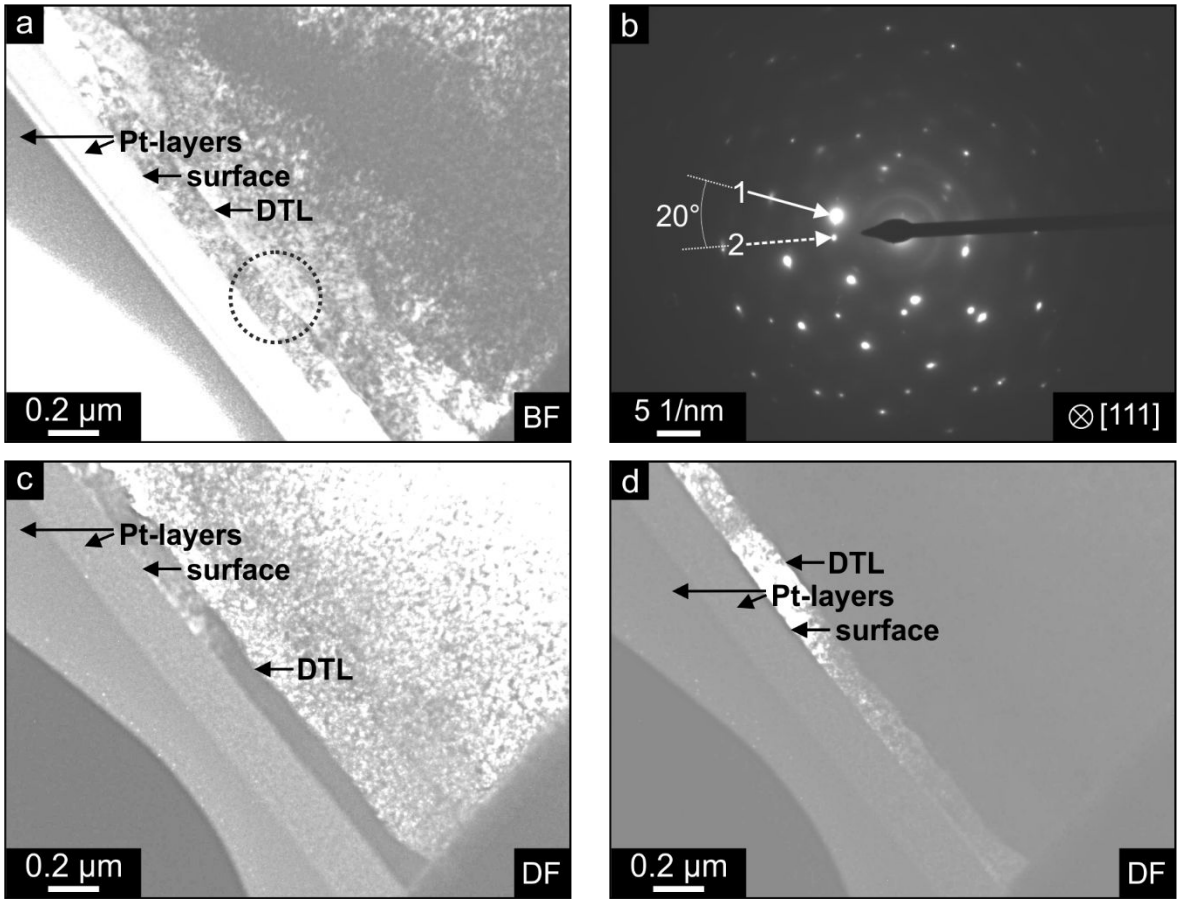

**Figure S5: Influence of the Hertzian contact pressure on the Hamilton stress field beneath the sliding spherical indenter for a friction coefficient of 0.34 and a contact radius of 57.61 µm.** (a) $p_{Hertz}$ = 719 MPa ($F_n$ = 5 N, $d_{sphere}$ = 10 mm), (b) $p_{Hertz}$ = 1439 MPa ($F_n$ = 10 N, $d_{sphere}$ = 5 mm). The shear stress components in normal/sliding direction ($\tau_{ND/SD}$) and three iso-lines, 0 MPa (dashed line), 5 MPa (continuous line) and 10 MPa (dotted line), are shown. The contact stresses are increased by a factor of two, by doubling the Hertzian contact pressure. This is why the position of the 5 MPa iso-line in (a) develops in that for 10 MPa in (b).

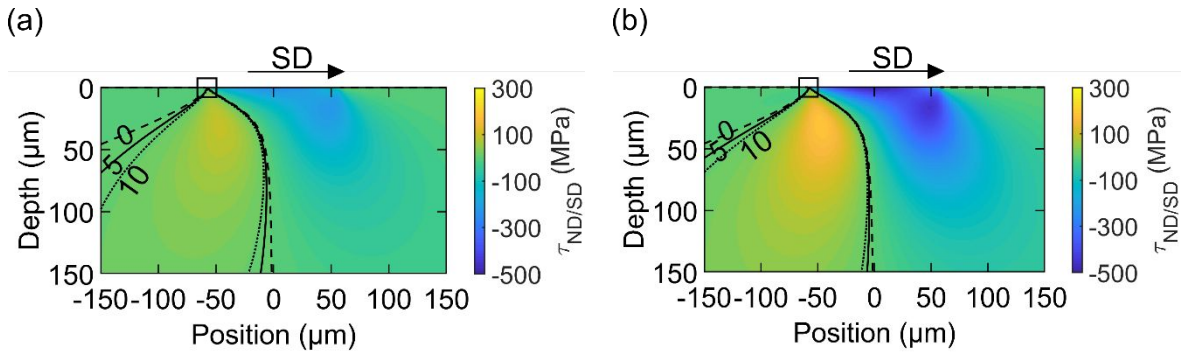


**Figure S6: Influence of the contact radius on the Hamilton stress field beneath the sliding spherical indenter for a friction coefficient of 0.34 and a Hertzian contact pressure of 1953 MPa.** (a) $r_{contact}$ = 78 µm ($F_n$ = 25 N, $d_{sphere}$ = 5 mm), (b) $r_{contact}$ = 156 µm ($F_n$ = 100 N, $d_{sphere}$ = 10 mm). The shear stress components in normal/sliding direction ($\tau_{ND/SD}$) and three iso-lines, 0 MPa (dashed line), 5 MPa (continuous line) and 10 MPa (dotted line), are shown. The stress field's dimension is increased by doubling the contact radius.

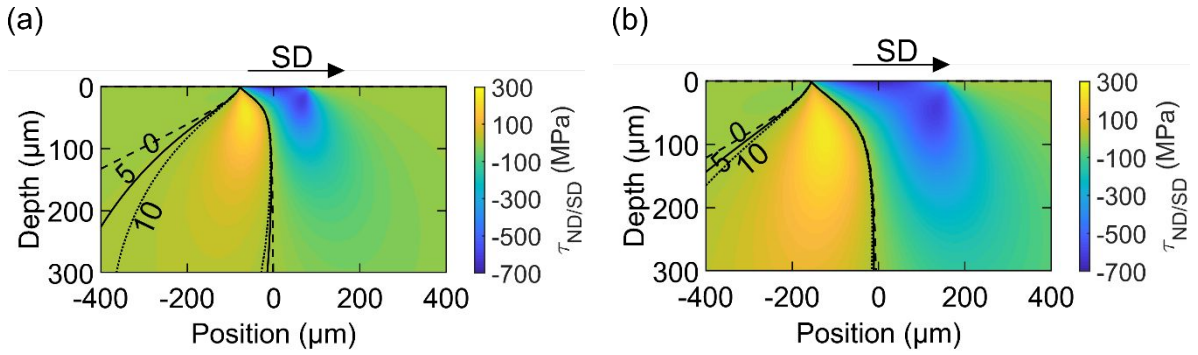

**Figure S7: Influence of the friction coefficient on the Hamilton stress field beneath the sliding spherical indenter for a Hertzian contact pressure of 1953 MPa ($F_n$ = 2 N, $d_{sphere}$ = 10 mm, $r_{contact}$ = 42 µm).** (a) µ = 0.1, (b) µ = 0.35. The shear stress components in normal/sliding direction ($\tau_{ND/SD}$) and three iso-lines, 0 MPa (dashed line), 5 MPa (continuous line) and 10 MPa (dotted line), are shown. The shape of the stress field is changed by varying the friction coefficient.

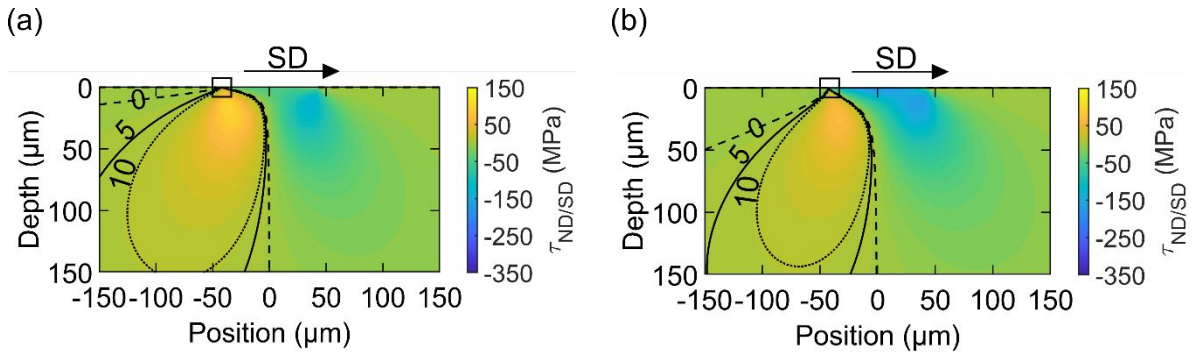


According to Hamilton [34,35], the Hamilton solution strongly depends on the Hertzian contact pressure, the contact radius, the friction coefficient and the Poisson ratio. Since the present work focuses on copper and sapphire, the Poisson ratio was constant, why its influence on the stress field is not considered here. By doubling the Hertzian contact pressure, keeping the contact radius and the friction coefficient constant, all the contact stresses are increased by a factor of two as well. This is shown in **Fig. S5**, where iso-stress lines for 0 MPa (dashed line), 5 MPa (continuous line) and 10 MPa (dotted line) are plotted as a function of depth under the contact. The position of the 5 MPa iso-line in **Fig. S5a** develops in that for 10 MPa in **Fig. S5b**, thereby approaching the surface compared to **Fig. S5a**. All the three dimensions in space expand, by increasing the contact radius. This is illustrated by the two dimensional stress field in **Fig. S6**, keeping in mind that the third dimension in space (perpendicular to the plane view) also increases. The friction coefficient modifies the shape of the stress field. Its severe influence on the stress field is illustrated in **Fig. S7**. According to Hamilton [34,35], for friction coefficients

greater or equal 0.34, the location of the maximum stress is exactly *at* the surface, whereas for lower friction coefficients it is located *underneath* the contact.